Cell Death & Differentiation (2020) 27:3337–3353
https://doi.org/10.1038/s41418-020-0581-5

Cell Death & Differentiation

ARTICLE

LRIK interacts with the Ku70–Ku80 heterodimer enhancing the efficiency of NHEJ repair

Dan Wang[1] · Zheng Zhou[1] · Erzhong Wu[2] · Can Ouyang[1] · Guifeng Wei[2,5] · Yunfei Wang[2] · Dandan He[2] · Ya Cui[2] · Dongdong Zhang[2] · Xiaomin Chen[2] · Simon H. Reed[3] · Jianjun Luo[2] · Runsheng Chen[2,4]

Received: 15 October 2019 / Revised: 10 June 2020 / Accepted: 12 June 2020 / Published online: 25 June 2020
© The Author(s), under exclusive licence to ADMC Associazione Differenziamento e Morte Cellulare 2020

Abstract

Despite recent advances in our understanding of the function of long noncoding RNAs (lncRNAs), their roles and functions in DNA repair pathways remain poorly understood. By screening a panel of uncharacterized lncRNAs to identify those whose transcription is induced by double-strand breaks (DSBs), we identified a novel lncRNA referred to as *LRIK* that interacts with Ku, which enhances the ability of the Ku heterodimer to detect the presence of DSBs. Here, we show that depletion of *LRIK* generates significantly enhanced sensitivity to DSB-inducing agents and reduced DSB repair efficiency. In response to DSBs, *LRIK* enhances the recruitment of repair factors at DSB sites and facilitates γH2AX signaling. Our results demonstrate that *LRIK* is necessary for efficient repairing DSBs via nonhomologous end-joining pathway.

Introduction

DNA damage induced by exogenous or endogenous factors is repaired by various DNA repair pathways, which are also components of the cellular DNA damage response (DDR) network. If damaged DNA cannot be repaired efficiently and accurately, it may cause mutations in the genetic material and lead to genomic instability. Such changes may cause alterations to the normal functioning of the cell by disrupting cell cycle, or the induction of apoptosis, and may result in the initiation and promotion of cancer development [1, 2]. Long noncoding RNAs (lncRNAs) have been known for many years, but their potential involvement in the DDR, and more specifically in DNA repair, is only now emerging. It has been reported that a certain number of lncRNAs play important roles in diverse biological pathways [3, 4]. In particular, it has been suggested that lncRNAs are engaged in the cellular DDR across a range of different signaling pathways it encompasses. For instance, *lincRNA-p21* [5, 6], *LincRNA-RoR* [7], *PANDA* [8], *DINO* [9], and Meg3 [10] are all induced by p53 upon DNA damage and interact with various different proteins to mediate cell cycle arrest and apoptosis; two important end points of the DDR.

Since DNA double-strand breaks (DSBs) are the most lethal forms of genetic damage in cells [11, 12], the repair of DSBs has been deeply investigated and broadly evaluated. Multiple proteins are engaged in two major repair pathways to restore damaged DNA sites, thus preventing chromosomal aberrations and cell death. The nonhomologous end-joining (NHEJ) pathway operates throughout the cell cycle, but is crucial within the G0 and G1 cell phases when DSBs are recognized and repaired by NHEJ.

Edited by R. A. Knight

Supplementary information The online version of this article (https://doi.org/10.1038/s41418-020-0581-5) contains supplementary material, which is available to authorized users.

✉ Zheng Zhou
zhouzheng@hnu.edu.cn

✉ Jianjun Luo
luojianj@ibp.ac.cn

✉ Runsheng Chen
rschen@ibp.ac.cn

[1] College of Biology, Hunan University, Changsha 410082, PR China

[2] Key Laboratory of RNA Biology, Institute of Biophysics, Chinese Academy of Sciences, Beijing 100101, PR China

[3] Division of Cancer and Genetics, School of Medicine, Cardiff University, Heath Park, Cardiff CF14 4XN, UK

[4] Guangdong Geneway Decoding Bio-Tech Co. Ltd, Foshan 528316, PR China

[5] Present address: Developmental Epigenetics, Department of Biochemistry, University of Oxford, South Parks Road, Oxford OX1 3QU, UK

During DSB repair by NHEJ, Ku70 plays a key role in conjunction with Ku80 to form the Ku70–Ku80 heterodimer. This complex has a preformed ring-like conformation that senses and binds the double-stranded ends of DSBs [13, 14]. Repair is initiated following the recruitment of the DNA-dependent protein kinase catalytic subunit (DNA-PKcs), which binds Ku separately. DNA-PKcs recruitment stabilizes Ku complex binding at the DSB and is the protein kinase responsible for signaling the presence of the DSB, by phosphorylating the histone variant H2AX to form gamma H2AX. This process marks the presence of the DSB and serves to recruit other DNA repair factors such as XRCC4-like factor (XLF), X-ray cross-complementing protein 4 (XRCC4), which together manifest as the repair foci [11, 15].

It was recently reported that in triple-negative breast cancer (TNBC) cell lines, lncRNA LINP1 is involved in DSB repair. They demonstrated that this lncRNA promotes efficient DSB repair possibly via interacting with Ku and DNA-PKcs where it serves as a scaffold [16]. Overexpression of LINP1 in these cells leads to significantly enhanced rates of NHEJ that causes the drug resistance to chemo and radiotherapy in TNBC cells. It is established that during the recognition of DSBs, the Ku heterodimer is able to bind different types of DSBs, including those with overhangs or blunt ends [17]. It is also known that the Ku heterodimer can bind with the RNA component of telomerase and assists in recruiting telomerase to telomeres [18–20]. Finally, we noted that prolonged binding of DNA repair factors at the sites of DSB's can trigger the DDR. Conceivably, cells coordinately regulate the transcription of specific lncRNAs, which mediate genome stability via the repair of DSBs by the NHEJ pathway, in response to DSB-inducing agent treatment.

Here, we report that repair of DSBs is regulated and enhanced by the damage-induced expression of a novel lncRNA we refer to as lncRNA interacting with Ku (*LRIK*, NONHSAG044790.2). Using a custom-designed microarray comprised of around 2000 uncharacterized lncRNAs, we screened for the presence of differentially expressed lncRNAs in response to cells treated with the DSB-inducing agent methyl methanesulfonate (MMS). *LRIK* interacts with the DSB recognition factor Ku heterodimer and enhances cellular resistance against DSB-inducing agents such as MMS, X-rays, and phleomycin. We also demonstrate that knockdown of *LRIK* significantly reduces the occupancy of Ku and its downstream factors on damaged chromatin. Depletion of *LRIK* reduces the efficient formation of DSB repair foci in a similar fashion to knockdown of Ku70 and Ku80, without affecting the induction of DSBs. Failure to sense the DSBs results in the impaired formation of γH2AX foci, reducing efficient DSB repair. Our data demonstrate that the interaction of *LRIK* with Ku enhances the binding of DSBs, promoting the efficient repair of damage by the NHEJ pathway.

Material and methods

Cell culture and transfections

HeLa, A549, and 293T cells were cultured in Dulbecco's Modified Eagle's Medium (Gibco) supplemented with 10% (v/v) Fetal Bovine Serum (Gibco) and 1% (v/v) Penicillin/Streptomycin (Gibco). MDA-MB-436 cells were cultured in RPMI 1640 medium (Gibco) supplemented with 10% (v/v) Fetal Bovine Serum (Gibco) and 1% (v/v) Penicillin/Streptomycin (Gibco). EJ5-GFP-U2OS and DR-GFP-U2OS cells were kind gifts of Prof. Xianlu Zeng (Northeast Normal University, China). All cells were tested for mycoplasma contamination by PCR. Human cells were transfected with reconstructed or unmodified plasmids by using Lipofectamine 2000 (Life Technologies) according to the manufacturer's instructions. Cells with a stable expression plasmid were selected by culture media with 1 μg/ml puromycin (Life Technologies).

Microarray samples and data analysis

Total RNA samples were extracted from untreated HeLa cells or treated with 0.005% MMS followed by 12 h of recovery. Microarray probes were designed against 1958 noncoding RNAs (ncRNAs). The custom-designed microarray platform was manufactured by Agilent with ID GPL23062 (Agilent-026619 Human ncRNA and mRNA array), consisting of probes for 1860 protein coding genes and 1958 lncRNA transcripts. LncRNA transcripts were collected from a number of different sources including our previous findings [21], unpublished data, as well as our database NONCODE [22] and so on. At least one probe was designed for each lncRNA transcript. Microarray sample preparation, hybridization, and data analysis were conducted as described previously [21]. The array data were subject to quality control and background subtraction by the GeneSpring software. Quantile normalization was modulated by limma package. The log2 fold change threshold, which defines significant transcription alteration in tested samples, was set to 1.5. MA plot was drawn with the R software.

Accession number

The microarray data related to this study have been deposited to the NCBI Gene Expression Omnibus with the accession code GSE94868.

RNA extraction, reverse transcription, and quantitative RT-PCR

Total RNA was extracted using TRIzol agent (Invitrogen) following the manufacturer's instructions. As for cytoplasmic and nuclear RNA extraction, cells were fractioned with the NE-PER Nuclear and Cytoplasmic Extraction Reagents (Thermo Scientific) to separate each fraction followed by isolating RNA with TRIzol agent. RNA was subjected to synthesize the first strand of cDNA with SuperScript III First-Strand Synthesis System for RT-PCR (Invitrogen) according to the manufacturer's procedure. Quantitative real-time PCR (qPCR) was conducted with UltraSYBR Mixture (Cwbio). qRT-PCR was performed with TransScript II Green One-Step qRT-PCR SuperMix (TransGen) according to the manufacturer's protocol when using RNA as the template. The primers used in qPCR are listed in Supplementary Table S1.

Rapid amplification of cDNA ends (RACE)

5′ RACE and 3′ RACE were conducted as manufacturer's instructions using FirstChoice RLM-RACE kit (Life Technologies). Primers used in RACE are listed in Supplementary Table S1. Briefly, for 5′ RACE, total RNA was treated with Calf Intestine Alkaline Phosphatase and Tobacco Acid Pyrophosphatase before an RNA Adapter (supplied by the manufacturer) was ligated to RNA by using T4 RNA ligase. Random-primed reverse transcription reaction was performed with SuperScript III First-Strand Synthesis System (Invitrogen). 5′ end of *LRIK* was amplified through nested PCR. For 3′ RACE, first-strand cDNA was generated from total RNA using the 3′ RACE Adapter (supplied by the manufacturer). Nested PCR was conducted to get the 3′ end of *LRIK*. All PCR products of RACE results were separated on 1.5% agarose gels. The bands were purified with the Gel and PCR Clean-Up System (A9282, Promega). The purified DNA was then cloned into the pGEM-T Vector Systems I (A3600, Promega) to retrieve the sequence. At least five colonies were sequenced for every RACE PCR.

Northern blot

Northern blot was performed using DIG Northern Starter Kit (Roche) following the manufacturer's protocol. DIG-labeled RNA probes were generated by in vitro transcription using T7 RNA polymerase (Roche) and digoxigenin-11-UTP (Roche). Briefly, 30 μg total RNA was applied to 1.2% (w/v) agarose electrophoresis in MOPS buffer. After separation, RNA transferred onto a positively charged nylon membrane (GE Life Sciences, RPN303B) through capillary blotting followed by cross-linking with UV. The membrane was pre-hybridized with an appropriate volume of DIG Easy Hyb at 68 °C for 30–60 min before conducting the hybridization with DIG-labeled RNA probes overnight at 68 °C. After washing with 2× SSC, 0.1% (w/v) SDS for 5 min twice at room temperature and 0.1× SSC, 0.1% (w/v) SDS for 15 min twice at 68 °C, CPD-Star detection reagent was applied to the membrane. The images were acquired by exposing the membrane to standard X-ray film.

RNA fluorescence in situ hybridization

Appropriate amounts of cells were seeded on glass coverslips the day before experiments. Tested samples were applied with 30 μg/ml phleomycin (ab143437, Abcam) or 5 μm doxorubicin for 2 h and recovery for 2 h. Then, samples were fixed with 4% (w/v) paraformaldehyde in PBS at the indicated times after the treatment. After samples were washed three times with PBS, they were incubated with pre-cold permeabilization buffer (1× PBS, 0.5% (v/v) Triton X-100) for 5 min at 4 °C. *LRIK* was detected with in vitro transcribed DIG-labeled RNA probe with a length of ~200 nt. Samples were incubated in hybridization buffer (50% (v/v) formamide, 5× SSC, 500 μg/μl yeast tRNA, 1× Denhardt's solution, 500 μg/ml herring sperm DNA, 50 μg/ml Heparin, 2.5 mM EDTA, 0.1% (v/v) Tween-20, 0.25% (w/v) CHAPS) at 65 °C for 20 min, and they were hybridized with DIG-labeled RNA probes in the same buffer 1 h at the same temperature. Coverslips with samples were washed five times with washing buffer (4× SSC, 0.1% (v/v) Tween-20) for 5 min. Then, all samples were washed with 2× SSC buffer once and 1× SSC buffer once. PBS buffer containing 3% (v/v) H_2O_2 was applied on washed coverslips with samples for 20 min followed by three times washing with TN buffer (0.1 M Tris-HCl pH7.5, 0.15 M NaCl). The samples were incubated for 30 min at room temperature in TNB blocking buffer (0.1 M Tris-HCl pH7.5, 0.15 M NaCl, 0.5% (w/v) blocking reagent), and then they were incubated for 30 min again after anti-DIG antibody (Abcam, ab51949) was added to the buffer. After samples were washed with TNT buffer, TSA solution (PerkinElmer Life and Analytical Sciences) was applied onto the samples and incubated for 5–10 min at room temperature. Protein detection and nuclear staining were performed as the protocol described. After samples were washed with TNT buffer (0.1 M Tris-HCl pH7.5, 0.15 M NaCl, 0.2% (v/v) Triton X-100) and PBS, they were blocked with 2% (w/v) BSA solution for 30 min at room temperature. The samples were incubated with primary antibodies overnight at 4 °C followed by incubations with appropriate secondary antibodies and NucBlue Live ReadyProbes Reagent (Life Technologies, R37605) for 1 h at room temperature. Samples were mounted onto clean glass slides with antifading agents (ProLong® Gold Antifade Reagent, Life P36930). The coverslips containing

samples were sealed with nail polish. Images were acquired using Olympus FluoView 1200 confocal microscope. The intensity and co-localization were calculated using ImageJ software.

Immunofluorescence

Appropriate amounts of cells were grown on glass coverslips the day before experiments. Cells were treated with 2 Gy of X-ray irradiation (MBR-1520R-3, X-ray-irradiation equipment, Hitachi) or 20 μg/ml phleomycin for 2 h, and were harvested at the indicated times. All collected samples were fixed with methanol at 4 °C for 1 h. Specimens were blocked in 2% (w/v) BSA for 60 min after they were gently washed three times in 1× PBS for 5 min. Samples were incubated with primary antibody anti-γH2AX (9718, Cell Signaling Technology, 1/400) overnight at 4 °C followed the incubation with fluorochrome-conjugated secondary antibodies (Goat anti-Rabbit IgG (H+L) Secondary Antibody, Alexa Fluor 488 conjugate, Life Technologies) and NucBlue Live ReadyProbes Reagent (Life Technologies) for 1 h at room temperature. Images were obtained by using Olympus FluoView 1200 confocal microscope.

Plasmid construction

Plasmids stably expressing shRNA were constructed based on commercial vector, pSliencer 2.0-U6 (AM5762, Ambion), according to the manufacturer's protocol. *LRIK* overexpression and *LRIK* antisense expression vector were constructed by inserting full-length cDNA of *LRIK* or antisense of *LRIK* into pCDH-CMV plasmid, respectively. The cDNA fragment of *X-ray repair cross-complementing protein 6* (*XRCC6*) and *XRCC5* was cloned into p3×Flag-CMV-10 vector (Sigma-Aldrich) following the manufacturer's protocol. pBABE HA-AsiSI-ER plasmid was provided generously by Prof. Xianlu Zeng (Northeast Normal University, China). pEJ5-GFP, pDR-GFP, and I-SceI plasmids were kindly given by Prof. Xingzhi Xu (Shenzhen University Health Science Center). Primers and shRNA used were listed in Supplementary Table S1.

Colony-forming assay

Prior to cell survival determination by colony-forming ability, plating efficiency of all cell lines had been measured. The appropriate number of cells from each cell line (500 *LRIK* knockdown HeLa cells; 500 *LRIK* rescued HeLa cells; 500 antisense of *LRIK* expression cells; 800 *LRIK* and BRCA1 knockdown HeLa cells; 1000 MDA-MB-436 cells) was added to petri dishes (10 cm), such that in each case ~200 colonies would form. Appropriate cells of samples were seeded for overnight and specimens were treated with X-ray-irradiation equipment (MBR-1520R-3, Hitachi) of a 2, 4, 6, 8 Gy dose, respectively. For phleomycin (ab143437, Abcam) or doxorubicin treatment, cells were treated at indicated concentrations for 2 h, respectively. Then, all samples were cultured in a CO_2 incubator. When colonies were formed after 10–14 days culture, cells were fixed using cold methanol and stained with 0.1% (w/v) crystal violet in 50% (v/v) methanol. The colonies were counted and normalized to plating efficiencies of untreated samples.

Neutral comet assay

Comet assays were conducted as previously described [23]. In brief, cells were treated with 20 μg/ml phleomycin for 2 h and were harvested either just after this treatment or after 2 h of recovery. Olympus FluoView 500 was used to observe acquired samples. The results were analyzed by CASP software and at least 100 cells were examined per condition for statistical analysis. The efficiency of DSB repair was calculated through the tail moment ratio, the mean tail length ratio and the Olive tail moment ratio between DNA from recovered (R) and phleomycin treated samples (D). R represents the samples treated with 20 μg/ml phleomycin for 2 h and recovered for 2 h. D represents the samples that treated with 20 μg/ml phleomycin for 2 h.

RNA pull-down assay

Biotinylated *LRIK*, antisense of *LRIK,* and truncated *LRIK* were generated by in vitro transcription with the Biotin RNA Labeling Mix (Roche) and T7 RNA polymerase (Roche) followed by RNase-free DNase I (Ambion) treatment and purification with NucleoSpin RNA Clean-up XS (Macherey Nagel). RNA pull-down assay was conducted according to the methods described in the literature [24, 25] without any modification. The proteins associated with RNA were subjected to 4–12% NuPAGE Bis-Tris gels (Life Technologies) followed by silver staining with SilverQuest Silver Staining Kit (Life Technologies) for further mass spectrometric analysis.

UV cross-linking RNA immunoprecipitation (UV-RIP)

The UV-RIP was carried out according to the protocol described in the publication [26]. CL1000 Ultraviolet Crosslinker (UVP) was used to conduct the cross-linking. The antibodies used in UV-RIP were anti-Flag (f3165, Sigma-Aldrich), anti-Ku70 (PLA0263, Sigma-Aldrich), anti-Ku80 (PLA0264, Sigma-Aldrich), anti-Ku80 (ab236277, Abcam), normal mouse IgG (sc-2025, Santa Cruz Biotechnology), and normal rabbit IgG (sc-2027, Santa Cruz Biotechnology). The retained samples were removed by proteinase K (Promega), and RNA of samples

was extracted with TRIzol reagent for further investigation. The samples were treated with DNase I and were subjected to qRT-PCR to detect the enrichment of *LRIK*.

Chromatin fraction preparation

Cells were treated with 150 μm phleomycin or 5 μm doxorubicin for 2 h. Samples without recovery time were harvested immediately after the treatment. For recovery samples, cells were cultured for additional 1 h in normal media after PBS washes. Harvested cells were washed with pre-cold PBS twice and samples were extracted twice in CSK buffer (100 mM NaCl, 300 mM sucrose, 3 mM $MgCl_2$, 0.7% (v/v) Triton X-100, 10 mM PIPES, pH7.0, 0.3 mg/ml RNase A (R4875, Sigma-Aldrich)) at 4 °C for 3 min. Samples extracted were washed with ice-cold PBS three times and stored in SDS-loading buffer for further analysis.

Western blot and antibodies

At indicated times, cells were washed with PBS. Whole cell extracts were acquired by homogenizing washed cells in 2× SDS-loading buffer. Extracts were boiled for 5 min. In brief, samples (20–80 μg) were resolved by 8% SDS-polyacrylamide gel (15% for histone H3 and γH2AX detection) electrophoresis and transferred to PVDF membranes (Millipore). The bands were quantified with ImageJ software. Primary antibodies used in this study were anti-β-actin antibody (60008-1-Ig, Proteintech, 1/5000), anti-H3 antibody (sc10809, Santa Cruz Biotechnology, 1/200), anti-phospho-histone H2AX (Ser139) antibody (9718, Cell Signaling Technology, 1/1000), anti-Ku70 antibody (PLA0263, Sigma-Aldrich, 1/1000), anti-Ku80 antibody (PLA0263, Sigma-Aldrich, 1/2000), anti-Ku80 (ab236277, Abcam, 1/1000), anti-DNA-PKcs antibody (sc5282, Santa Cruz Biotechnology, 1/200), anti-XRCC4 antibody (15817-1-AP, Proteintech, 1/1000), anti-ATM antibody (2873S, Cell Signaling Technology, 1/2000), anti-ATR antibody (2790S, Cell Signaling Technology, 1/2000), and anti-Flag antibody (f3165, Sigma-Aldrich, 1/5000). HRP-conjugated anti-rabbit IgG (7074, Cell Signaling Technology, 1/2000) and anti-mouse IgG (7076, Cell Signaling Technology, 1/2000) were the secondary antibodies.

Chromatin immunoprecipitation (ChIP) assay

ChIP assays were carried out as described previously [27] with slight modifications. The AsiSI-HeLa cells were treated with 300 nM 4-OHT for 4 h to induce DSBs. Formaldehyde was added to the medium at a final concentration of 1% and incubated for 10 min at room temperature. Glycine was added to a final concentration of 0.125 M to stop the reaction. Then cells were washed with cold PBS and harvested by scraping. Pelleted cells were incubated in ChIP lysis buffer (50 mM Tris pH8.1, 10 mM EDTA, 1% SDS) for 10 min before sonicated eight times for 10 s, so as to shear DNA to an average fragment size of about 500–1000 bp. Samples were diluted ten times in dilution buffer (0.01% SDS, 1.1% Triton X-100, 1.2 mM EDTA, 16.7 mM Tris pH8.1, 167 mM NaCl) and precleared with previously blocked Protein A/G beads (Life Technologies) for 3 h at 4 °C. The beads were blocked with BSA and herring sperm DNA. Precleared samples were incubated overnight with 2-μg-specific antibodies at 4 °C. Add 20 μl Protein A/G beads and incubated for another 4 h at 4 °C following with washing beads in dialysis buffer (2 mM EDTA, 50 mM Tris pH8.0, 0.2% SDS) once and in wash buffer (100 mM Tris pH8.8, 500 mM LiCl, 1% NP-40, 1% NaDoc) for four times. Add 100 μl of elution buffer and incubation for 15 min. Repeat the elution process once and then adding NaCl and incubating overnight at 65 °C to reverse the cross-link. After RNase A and proteinase K treatment, DNA was purified with phenol/chloroform and analyzed by qPCR. The primers used located in proximity to (200 bp) and distal (2 Mb) from the AsiSI site on chromosome 22 at position 20850307 (GRCh37/hg19). The antibodies used are anti-Ku70 antibody (ab83501, Abcam), anti-Ku80 antibody (2753, Cell Signaling Technology), anti-DNA-PKcs antibody (ab168854, Abcam), and anti-XRCC4 antibody (15817-1-AP, Proteintech).

DSB repair assays

To qualify the DSB repair by NHEJ and HR after *LRIK* knockdown or overexpression, U2OS EJ5-GFP and DR-GFP cells were transfected with indicating shRNA plasmids or overexpression plasmids, then cells were transfected with I-SceI plasmid after 24 h. For HeLa cells, shNeg, sh*LRIK*-2, and sh*LRIK*-3 cells or *LRIK* overexpression cells were transfected with pEJ5-GFP or pDR-GFP plasmids, and 24 h later cells were transfected with I-SceI plasmid. Cells were suspended in PBS buffer after 48 h and the NHEJ or HR efficiencies were determined by flow cytometry (FACS-Calibur or LSRFortessa, Becton Dickinson, USA). Twenty thousand cells of each sample were tested and data were analyzed with FlowJo software.

Protein purification and electrophoretic mobility shift assay (EMSA)

The protein used in the EMSA was expressed in *E. coli* DL21 (DE3) by using pET-28a expression vector. After transfection, the bacteria were incubated until reaching 0.6 at OD600. Then, the recombinant protein was induced by adding 1 mM IPTG for overnight at 16 °C. Next, the protein was purified with His-tag protein purification kit (Beyotime,

P2226) following the manufacturer's protocol. In brief, *E. coli* lysate containing overexpressed Ku70 was incubated with BeyoGold™ His-tag Purification Resin for 30 min. The resin was then eluted eight times with elution buffer after washing four times with the washing buffer.

Full length of *LRIK* was labeled with biotin through in vitro transcription assays. The EMSA was conducted as pervious report [28]. 0.7 pmol of biotinylated *LRIK* was used for each reaction. The secondary structure of *LRIK* was formed by heating at 95 °C for 5 min following with slowly cooled down to room temperature. The indicated amount of purified protein and biotinylated *LRIK* was incubated in binding buffer (100 mM HEPES pH7.5, 200 mM KCl, 10 mM $MgCl_2$, 10 mM DTT) for 30 min at room temperature. The mixtures were subjected to electrophoresis on a 6% nondenaturing polyacrylamide 0.5x TBE gel. The gel was then transferred to a nylon membrane and imaged by incubation with Chemiluminescent Nucleic Acid Detection Module Kit (Thermo #89880).

Chromatin isolation by RNA purification (ChIRP)

The ChIRP assays were performed as previous described [29]. Briefly, the ChIRP probes were designed at Biosearch Technologies. Cells were transfected with AsiSI plasmid before cross-linking with 0.5 mg/ml AMT [30, 31]. Then cells were exposed at 350 nm UV for 10 min on ice followed by cell lysis (lysis buffer: 50 mM Tris-Cl pH7.0, 10 mM EDTA, 1% SDS) and sonication. Samples were sonicated in a 4 °C water bath with 10 s ON, 10 s OFF pulse intervals and sonication time was set for 15 min. Sonicated specimens were hybridized with 100 pmol biotinylated probes in hybridization buffer (750 mM NaCl, 1% SDS, 50 mM Tris-Cl pH7.0, 1 mM EDTA, 15% formamide, PMSF, P.I. and RNase inhibitor) at 37 °C for 4 h and C-1 magnetic beads were added. After incubation at 37 °C for 30 min, beads were collected and washed with wash buffer (2×SSC, 0.5% SDS, PMSF) for five times. RNA contained in washed samples was isolated with TRIzol and the enrichment of *LRIK* was examined. DNA contained in washed samples was eluted and purified with phenol/chloroform. The enrichments of the specific DNA fragments were detected with RT-qPCR by using the primers located in proximity to (60 bp) and distal (2 Mbp) from the AsiSI site on chromosome 22 at position 20850307 (GRCh37/hg19). The probes used in ChIRP are listed in Supplementary Table S1.

Statistics

The precise number of samples in each experiment was indicated in figure legends. Except for specific indications, data are expressed as mean ± standard deviation (SD) and the statistical significance was determined by two-tailed Student's *t*-test. Significance was referred as $*P < 0.05$, $**P < 0.01$, and $***P < 0.001$.

Results

Identification of upregulated lncRNAs following induction of DSBs

Since the transcription of many ncRNAs is often associated with their cellular roles [4], we reasoned that ncRNAs involved in the DDR may also be transcribed following exposure of cells to DNA damaging agents. To identify candidate ncRNAs expressed in response to DNA damage, custom-designed ncRNA microarrays with collections of ncRNAs including self-discovered ncRNAs, which have been deposited into the NONCODE database [22], were applied for the detection of damage-induced ncRNAs in HeLa cells, following their treatment with MMS, a DSB-inducing chemical (Fig. 1a). Following the experimental validation of the expression changes upon MMS treatment using qPCR (Fig. 1b), a novel lncRNA (NONCODE Gene ID: NONHSAG044790.2, Transcript ID: NONHSAT114847.2), which we named as *LRIK*, was selected as a candidate for further investigation based on its relatively higher expression level of induction following exposure to MMS. This chemical can induce various types of DNA damage, including DNA DSBs. Therefore, to test whether enhanced transcription of *LRIK* is primarily induced by DSBs, we repeated these experiments using other DSB-inducing genotoxic agents, including X-rays and phleomycin [32]. In addition, we repeated these experiments treating a variety of different cell lines, to confirm that the observations are not unique to HeLa cells (Fig. 1c–f).

Increased expression of *LRIK* following induction of DSBs was also examined cytologically by single-molecular RNA fluorescence in situ hybridization (RNA FISH) assay in HeLa cells, following their exposure to 30 μg/ml of phleomycin (Fig. 1g) or doxorubicin (Supplementary Fig. S1). Collectively, these results show that the transcription of *LRIK* is significantly elevated in response to DSB-induced stress in human cells.

Characterization of LRIK and identification of its interacting partners

In human cells, *LRIK* is a transcript located on chromosome 6 (127296102–127296760; GRCh38/hg38) (Fig. 2a). Northern blotting analysis revealed a transcript with a length about 600 nucleotides (Fig. 2b), which coincides well with the results of RACE assays (Supplementary

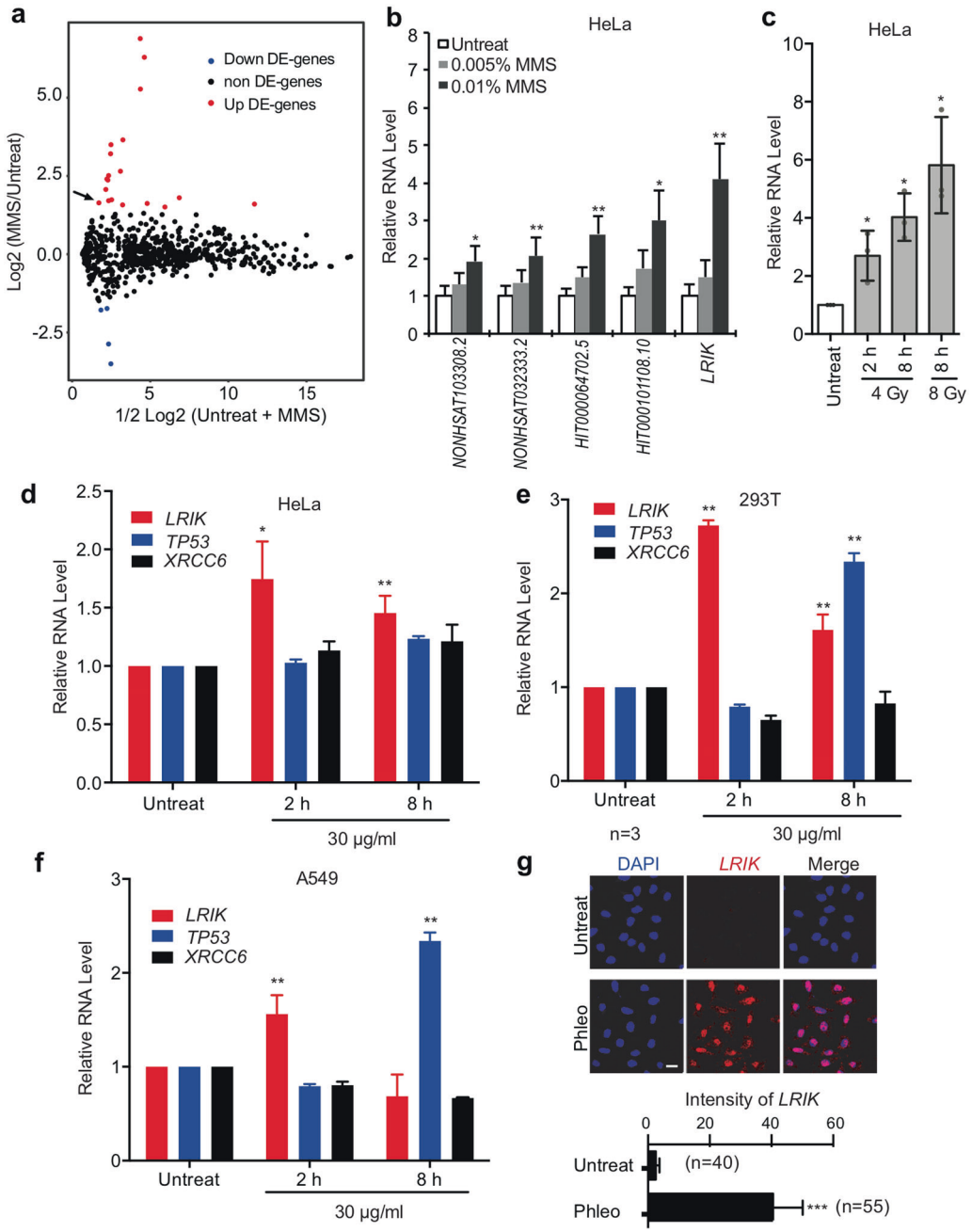

Fig. 1 Transcription induction of *LRIK* in response to DNA damage. a MA plot of long noncoding RNAs tested in custom-designed microarrays. Black dots: non-differentially expressed genes (non-DE genes); red dots: upregulated differentially expressed genes (up DE genes) identified in this study; blue dots: downregulated differentially expressed genes (down DE genes) identified in this study. The arrow indicates *LRIK*. **b** Validation of transcription induction of lncRNAs listed by using qRT-PCR. RNAs were extracted from HeLa cells treated with MMS. The error bars indicate SD ($n = 3$ independent experiments). **c** qRT-PCR analyses in HeLa cells show *LRIK* was upregulated under 4 or 8 Gy of X-ray irradiation. The error bars indicate SD ($n = 3$ independent experiments). **d** Elevated transcriptions of *LRIK* were observed in HeLa cells treated with phleomycin. **e** Transcription induction of *LRIK* in response to phleomycin induced DNA damage stress in 293T cells. **f** Transcription induction of *LRIK* in response to phleomycin induced DNA damage stress in A549 cells. *TP53* and *XRCC6* were used as positive and negative control, respectively, in (**d**–**f**). The error bars indicate SD (**d**: $n = 3$, **e**: $n = 3$, **f**: $n = 3$, independent experiments). **g** FISH results showed that *LRIK* was upregulated in phleomycin treated cells compared with untreated HeLa cells. Cells were fixed after the treatment of 30 μg/ml phleomycin for 2 h and recovery for 2 h, then samples were immunostained with *LRIK* probe (red) and DAPI (blue). The intensity of *LRIK* is shown below ($n = 3$ independent experiments, the precise number of cells analyzed in total per condition was indicated). Scale bar, 20 μm. $^*P < 0.05$, $^{**}P < 0.01$, $^{***}P < 0.001$, by two-tailed Student's *t* test.

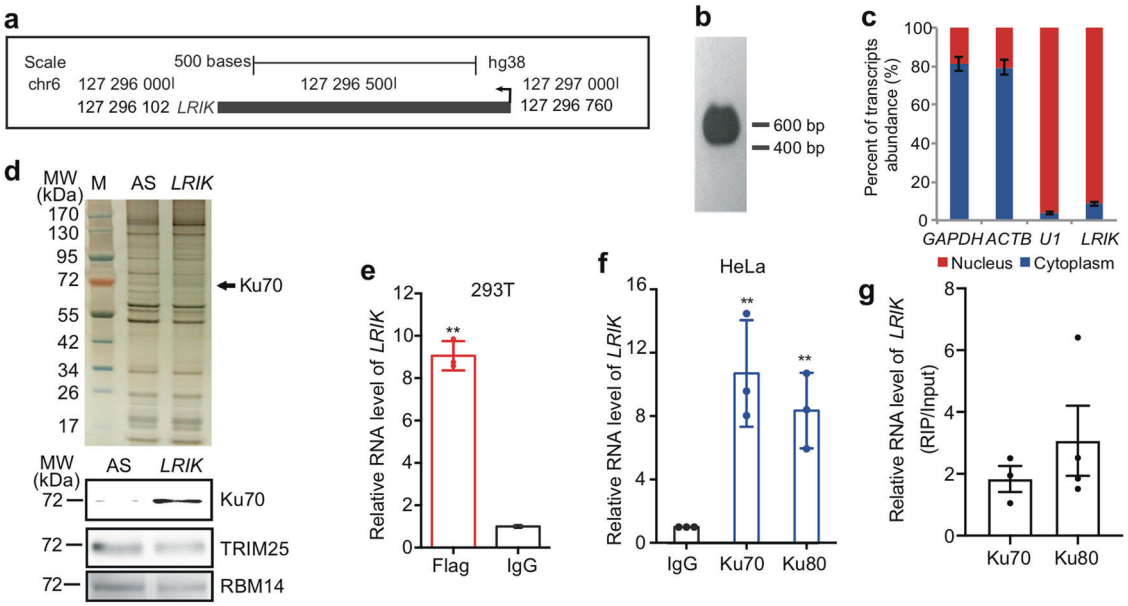

Fig. 2 ***LRIK* interacts with the DSB repair component Ku70. a** The transcription region of *LRIK*. **b** The representative image of Northern blotting assay. *LRIK* was detected with DIG-labeled RNA probes and 30 µg total RNA sample was loaded. **c** Cellular distribution of *LRIK*. Listed RNAs were measured by qRT-PCR after cell fractionation. The error bars indicate SD (for U1, $n = 4$, for the other conditions, $n = 5$ independent experiments). **d** Top, pull-down assays were performed by using biotin labeled *LRIK* (7 pmol) incubated with HeLa nuclear extracts (1 mg) to enrich proteins binding with *LRIK*. The retrieved proteins were subjected to NuPAGE Bis-Tris gels followed by silver stain and mass spectrometric identification. The arrow indicates Ku70 as the binding candidate interacting with *LRIK* in vitro. Bottom, western blotting analyses following pull-down assays showed the specific interaction between *LRIK* and Ku70. AS indicates antisense of *LRIK*. **e** UV cross-linking RIP results show that *LRIK* was enriched by Ku70-Flag in 293T cells with overexpression of a Flag epitope-tagged Ku70. RNA was immunoprecipitated with anti-Flag antibody followed by detecting *LRIK* and *U1*. The relative enrichment was calculated as RNA associated with Flag IP relative to the *U1* RNA. IgG was used as a negative control. The error bars indicate SD ($n = 3$ independent experiments). **f** UV cross-linking RIP with anti-Ku70 or anti-Ku80 antibodies (Sigma-Aldrich) confirmed that *LRIK* interacts with Ku heterodimer in vivo. Co-immunoprecipitation ncRNAs with anti-Ku70 or anti-Ku80 antibodies, respectively, in HeLa cells were detected with qRT-PCR. The error bars indicate SD ($n = 3$ independent experiments). $^*P < 0.05$, $^{**}P < 0.01$, by two-tailed Student's t test. **g** The results of UV cross-linking RNA IP by anti-Ku80 (Abcam) in HeLa cells. RNA was immunoprecipitated with indicated antibodies followed by detecting *LRIK*. The relative enrichment was calculated as RNA associated with Ku70/Ku80 IP relative to the input. There is no significant difference between Ku70 IP and Ku80 IP results ($P = 0.413$). The error bars indicate SEM.

Fig. S2a). *LRIK* has no coding capacity, as predicted by CPAT [33] and Coding-Noncoding Index (CNCI) [34] (CNCI score: −0.1500472) (Supplementary Fig. S2b).

Quantitative RT-PCR assay on both the cytosolic and nuclear fractions revealed the nuclear location of *LRIK*. In contrast to *GAPDH* and *ACTB* but similar to *U1*, *LRIK* is mainly located in the cell nucleus (Fig. 2c). To further validate the subcellular localization of *LRIK*, FISH assay was employed. It was observed that the vast majority of *LRIK* is located in the nucleus (Supplementary Fig. S2c). Collectively, these results are consistent with *LRIK* playing a role in the cellular response to DNA damage.

Previous reports have shown that lncRNAs can bind with a protein partner(s) functioning coordinately. Therefore, we tested whether *LRIK* binds to protein(s) involved in the DDR. To do this, RNA pull-down assays were conducted to discover potential binding protein(s). Biotinylated sense or antisense transcripts of *LRIK* were incubated with nuclear extracts to enrich for *LRIK* associated protein(s), whose identities were subsequently characterized by mass spectroscopy (Supplementary Table S2). Among those, Ku70 (*XRCC6*) was hence identified as a potential binding partner of *LRIK* (Fig. 2d, top). Western blot analysis following RNA pull-down confirmed the specific interaction of *LRIK* with Ku70 as compared with the one observed using the antisense transcript of *LRIK* (Fig. 2d, bottom). To further confirm the interaction between *LRIK* and Ku70, cell lysates from Flag-Ku70 overexpressing 293T cells were examined using the UV-RIP assay. The results clearly confirmed the interaction between Ku70 and *LRIK* (Fig. 2e and Supplementary Fig. 2d). Besides, to confirm the direct interaction between *LRIK* and Ku70, we performed EMSA by using purified Ku70 and biotinylated RNA (Supplementary Fig. S2e, f). Our data showed free *LRIK* RNA bands decreasing and Ku-RNA shift bands increasing depend on the increased amount of Ku70 protein mixed with *LRIK* samples. Collectively, these results demonstrate that *LRIK* interacts specifically with Ku70.

It is known that Ku70 interacts with Ku80 to form the Ku heterodimer [11], which functions as a complex in the

NHEJ pathway. To verify the interaction between *LRIK* and the Ku complex in vivo, the UV-RIP assays were performed with anti-Ku70 and anti-Ku80 antibody, respectively. The results showed that *LRIK* enrichments obtained by these antibodies were significantly higher than that by IgG (Figs. 2f and S2g). To further confirm it, we repeated the UV-RIP assays with anti-Ku70 and anti-Ku80 antibody produced by different company (Abcam) and obtained similar results as showed in Fig. 2g (Supplementary Fig. S2h). Together, these observations demonstrate the association between *LRIK* and the Ku70–Ku80 heterodimer.

Expression of *LRIK* regulates the efficiency of DSB repair

Since *LRIK* binds to Ku heterodimer, which is responsible for the sensing of DNA DSBs during NHEJ, we next tested whether *LRIK* affects the repair of DSBs. Two *LRIK* knockdown HeLa cell lines were generated by using pSilencer plasmids (Fig. 3a) via shRNA strategy. The neutral comet assay was used to measure the efficiency of DSB repair in control (shNeg) and *LRIK* knockdown cells. Following phleomycin treatment, long comet tails indicated that DNA damages were generated in control (shNeg) cells and in *LRIK* knockdown cells (Fig. 3b). Notably, quantifying these data demonstrated that initial levels of DSB induction were not affected by *LRIK* depletion (Fig. 3c). After 2 h of recovery following phleomycin treatment, the rate of DSB repair as measured by tail moment (Fig. 3d), mean tail length, and Olive tail moment (Supplementary Fig. S3a, b) demonstrated that the DSB repair efficiency in *LRIK* knockdown cells was lower than that of control (shNeg) cells. Our data demonstrate that *LRIK* interacts with Ku70 during the DSB repair process and influences the efficiency of repairing DSBs.

Since inefficient repair of DSB lesions results in cell death, the cellular survival rates of cell lines were determined using the colony-forming assay to confirm the effect of *LRIK* on DSB repair efficiency. Compared with the control (shNeg) cell line, the *LRIK* knockdown cell lines exhibited significantly increased sensitivity to X-ray irradiation (Fig. 3e). Similarly, we also observed significantly reduced survival of *LRIK* knockdown cells following their treatment with phleomycin (Fig. 3f) or doxorubicin (Supplementary Fig. S3c). Overexpression of *LRIK* in *LRIK* knockdown cells rescued their sensitivities to phleomycin (Fig. 3f, g), demonstrating that efficient DSB repair requires sufficient levels of *LRIK*. To further investigate the role of *LRIK* in DSB repair, the dependence on *LRIK* for DSB repair was examined by analyzing the sensitivity of cells deficient in other HR factors. Knockdown of BRCA1 results in enhanced sensitivity of *LRIK* knockdown cells (Supplementary Fig. S3c, d). Moreover, after knocking down *LRIK* in BRCA1 defective cells (MDA-MB-436), increased sensitivity to phleomycin (Supplementary Fig. S3e, f) was conferred. This result indicates that *LRIK* functions in the Ku70 initiated DSB recognition process and is required for efficient DSB repair.

In order to explore the functional significance of *LRIK* in DSB repair, we examined the effect of *LRIK* on the repair efficiency of two major DSB repair pathways, NHEJ and HR, by using EJ5-GFP and DR-GFP systems, respectively [35, 36]. Cells containing the EJ5-GFP reporter can only repair DSB in the reporter plasmid by NHEJ and display GFP fluorescence following repair of DSB. Similarly, cells infected with the DR-GFP reporter only exhibit GFP fluorescence after DSB induced in the plasmid has been repaired by HR. Our data showed that knockdown of *LRIK* in EJ5-GFP reporter containing cells caused a significant reduction of the GFP-positive cells compared with the control sample (Fig. 3h), whereas knockdown of *LRIK* exhibited little effect on HR repair when evaluated using the DR-GFP system (Fig. 3i). Moreover, to address whether overexpression of *LRIK* could enhance the repair efficiency of NHEJ, we employed EJ5-GFP reporter assays to measure NHEJ efficiency in both *LRIK* overexpressed and normal cells (Fig. 3j). It indicates that *LRIK* overexpressed cells display a significantly increased NHEJ efficiency compared with the control cells. Together, these results indicate that *LRIK* is required for efficient repair of DSBs specifically through the NHEJ pathway.

LRIK enhances the binding of the Ku complex on damaged chromatin

Next, we examined the mechanism by which the interaction of *LRIK* with the Ku heterodimer enhances DNA DSB repair efficiency. It has been suggested that the early and prolonged binding of repair factors is crucial for the initiation and signaling of DNA damage and its repair [37]. The repair factors, which include DNA-PKcs, XRCC4, DNA Ligase IV, and XLF, bind to DSBs following the sensing of the damage by the Ku70–Ku80 heterodimer [17]. Therefore, we investigated whether *LRIK* influences the binding of the Ku70–Ku80 heterodimer and its binding partners on damaged chromatin following the induction of DSBs.

We extracted the chromatin fractions from the control (shNeg) cells and *LRIK* knockdown cells to examine the occupancy of tightly associated proteins with chromatin after exposing them to phleomycin or doxorubicin. Following the treatment with DSB-inducing agents, significantly increased chromatin occupancies of these factors were observed in control (shNeg) cells immediately after the treatments and following recovery for 1 h (lanes 1–3, Figs. 4a and S4a). However, compared with control

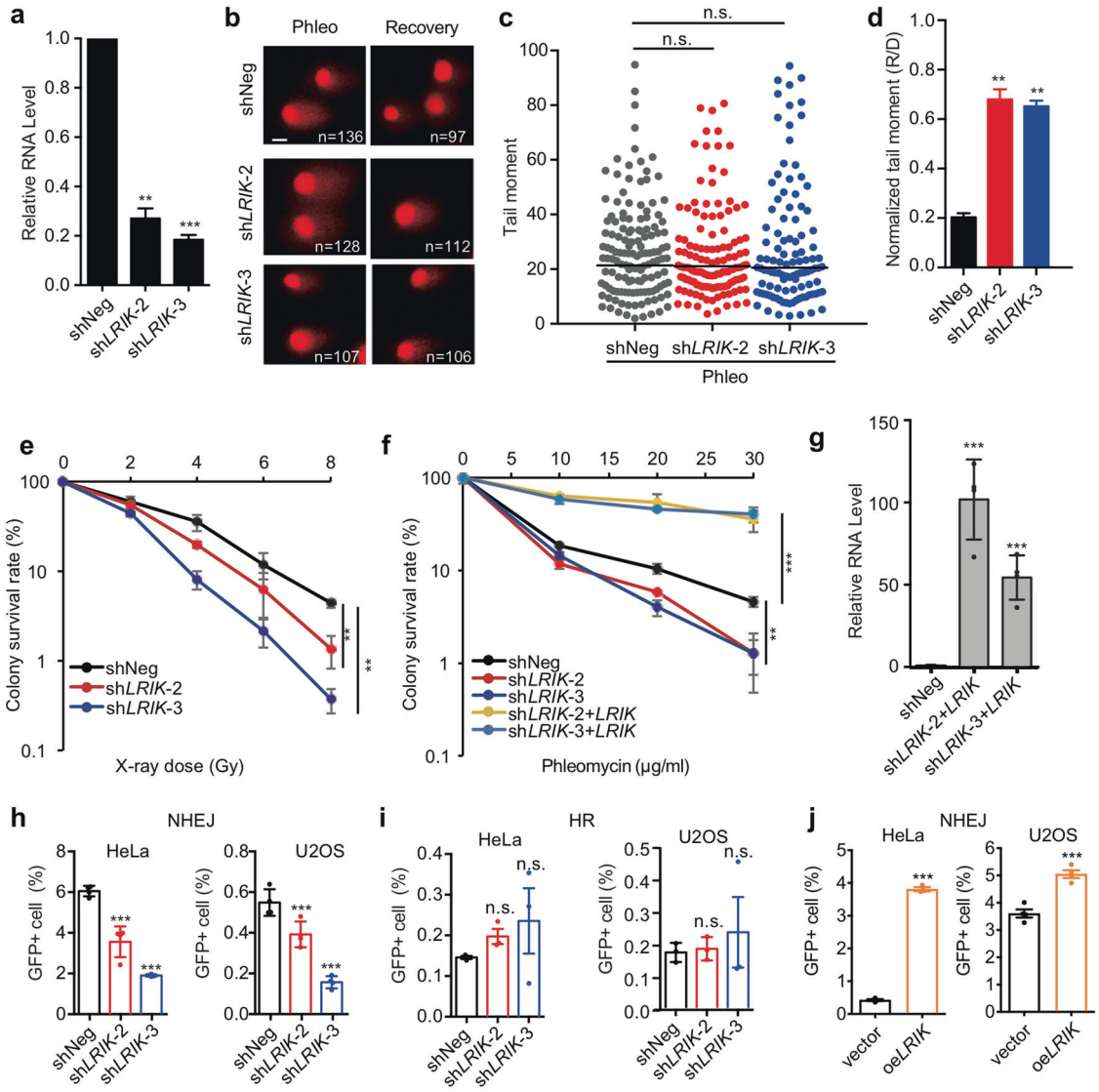

Fig. 3 ***LRIK* is essential for efficient repair of DSBs in human cells.** **a** The RNA level of *LRIK* in *LRIK* knockdown cells measured by qRT-PCR assay. The error bars indicate SD ($n = 6$ independent experiments). **b** Representative images of comet assays displayed reduced DSB repair efficiency in *LRIK* knockdown cells compared with control cells ($n = 3$ independent experiments, the precise number of cells analyzed in total per condition was indicated). **c** Tail moment of cells that treated by phleomycin without recovery was shown in column scatter plot with a line at geometric mean. ns not significant (pooled data from $n = 3$ independent experiments are shown). **d** Quantified tail moment of tested samples with CASP software showed significantly impaired DSB repair efficiency in *LRIK* knockdown cells. D represents samples that were treated with 20 μg/ml phleomycin for 2 h. R represents samples that were treated with 20 μg/ml phleomycin for 2 h and recovered for another 2 h. The error bars indicate SD ($n = 3$ independent experiments, the precise number of cells analyzed in total per condition was indicated in (**b**)). **e** Colony-forming assays showed that *LRIK* knockdown cells display increasing radiosensitivity compared with control shRNA (shNeg) cells. The error bars indicate SD ($n = 3$ independent experiments). **f** Colony-forming assays showed that knockdown of *LRIK* repressed the survival abilities following their treatment with phleomycin for 2 h at indicated concentrations and that can be rescued by overexpression of *LRIK*. The error bars indicate SD ($n = 3$ independent experiments). **g** The RNA level of *LRIK* after overexpressing *LRIK* in knockdown cells. The error bars indicate SD ($n = 4$ independent experiments). **h** NHEJ-mediate repair was analyzed in HeLa *LRIK* knockdown cells or U2OS *LRIK* knockdown cells by an EJ5-GFP reporter (mean ± SD, $n = 4$ independent experiments). **i** HR-mediate repair was analyzed in HeLa *LRIK* knockdown cells or U2OS *LRIK* knockdown cells by a DR-GFP reporter (mean ± SEM, $n = 3$ independent experiments). **j** NHEJ-mediate repair was analyzed in HeLa *LRIK* overexpression cells or U2OS *LRIK* overexpression cells by an EJ5-GFP reporter (mean ± SEM, $n = 3$ independent experiments for HeLa cells and $n = 4$ independent experiments for U2OS cells). Vector means overexpression of empty pCDH vector in cells, and oe*LRIK* means overexpression of pCDH-*LRIK* in cells. $^*P < 0.05$, $^{**}P < 0.01$, $^{***}P < 0.001$, by two-tailed Student's *t* test.

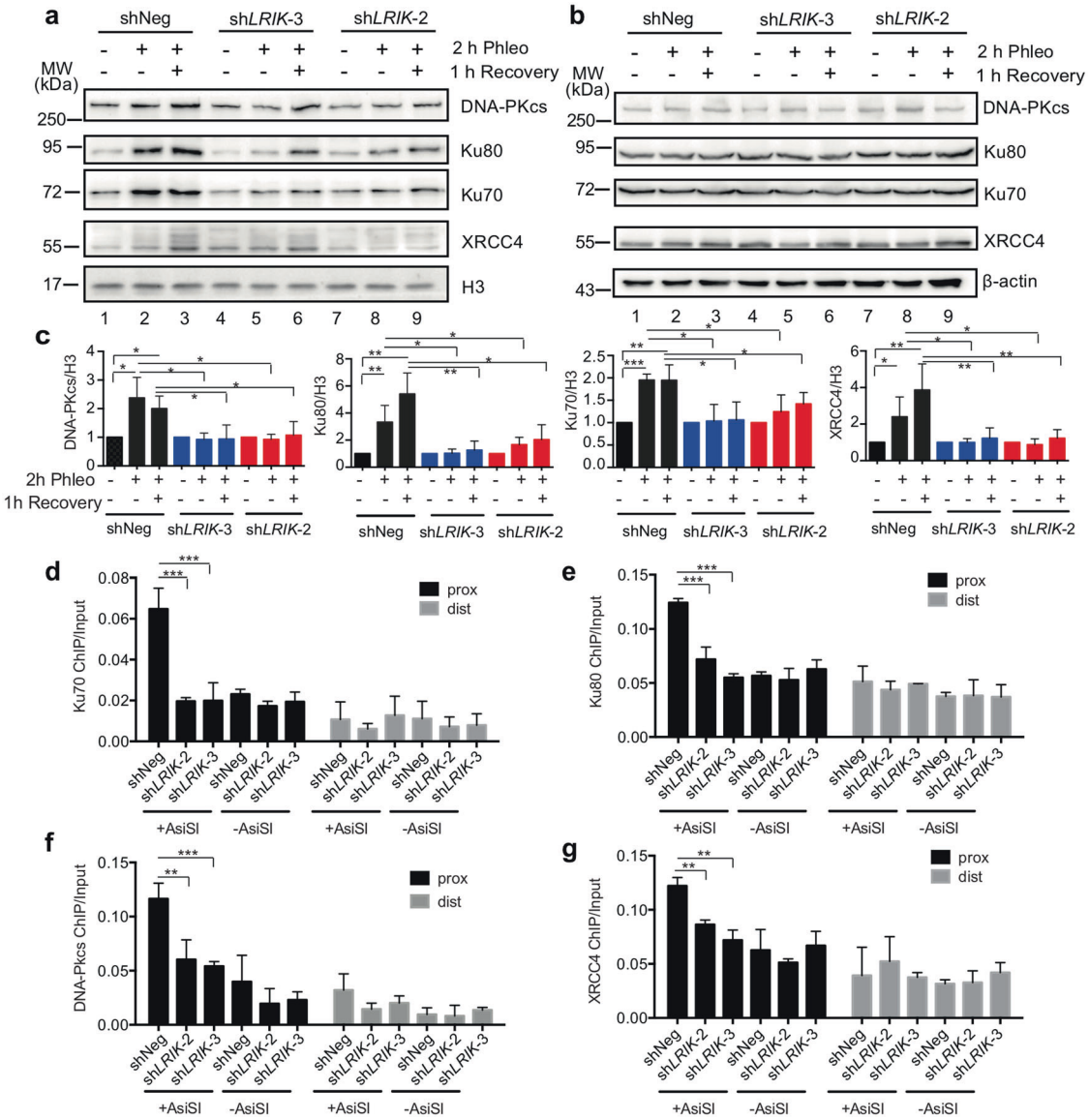

Fig. 4 *LRIK* enhances the occupancy of repair factors, including Ku70, Ku80, DNA-PKcs, and XRCC4, on damaged chromatin. a The representative image of western blotting analyses of chromatin fractions. The samples were extracted from *LRIK* knockdown and control shRNA (shNeg) cells that were treated with 150 μm phleomycin for 2 h with or without recovery for 1 h after treatments. **b** The representative image of western blotting analyses of whole cell extractions. Whole cell extractions were extracted from cell lines with the same treatments described in (**a**). **c** The relative band intensity histograms of chromatin fractions showed that knockdown of *LRIK* impaired the DSB repair factors, including Ku70, Ku80, DNA-PKcs, and XRCC4 binding with damaged chromatin. The results are shown as the ratio of target protein/H3. The error bars indicate SD (for Ku80 and XRCC4, $n = 4$, for DNA-PKcs and Ku70, $n = 3$ independent experiments). Accumulations of Ku70 (**d**), Ku80 (**e**), DNA-PKcs (**f**), and XRCC4 (**g**) at the indicated locus by ChIP assays performed in AsiSI cut cells (+AsiSI) and no AsiSI cut cells (−AsiSI). The bar plots show the enrichment relative to the input DNA, as detected with primers in the proximity or distal of the AsiSI-induced DSB. The error bars indicate SD ($n = 3$ independent experiments). ns not significant. $^*P < 0.05$, $^{**}P < 0.01$, $^{***}P < 0.001$, by two-tailed Student's *t* test.

(shNeg) cells, the increase in occupancy of Ku70, Ku80, DNA-PKcs, and XRCC4 on chromatin in the two *LRIK* knockdown cells was significantly reduced both immediately after phleomycin treatment (Fig. 4a compares the lanes 5 and 8 with lane 2; Fig. 4c shows histograms for the relative band intensities) and following 1 h of recovery (Fig. 4a compares the lanes 6 and 9 with lane 3; Fig. 4c shows histograms for the relative band intensities). Similarly, the reduced occupancy of Ku70, Ku80, DNA-PKcs, and XRCC4 on chromatin was also revealed in *LRIK* knockdown cells after doxorubicin treatment (Supplementary Fig. S4a, c). Importantly, the total protein levels of Ku70, Ku80, DNA-PKcs, and XRCC4 remained stable in control (shNeg) cells and *LRIK* knockdown cells following treatment with DSB-inducing agents (phleomycin and doxorubicin) either immediately after or following 1 h of

repair (Figs. 4b and S4b). This demonstrates that knockdown of *LRIK* does not inhibit the expression of Ku70, Ku80, DNA-PKcs, and XRCC4, suggesting that reduced binding of these factors is a direct result of reduced levels of cellular *LRIK* levels (Figs. 4 and S4).

To test whether knockdown *LRIK* influences the occupancy of Ku70, Ku80, XRCC4, and DNA-PKcs at DSB sites, ChIP assays were performed in control cells and *LRIK* knockdown cells with site-directed breaks introduced by AsiSI (Fig. 4d–g). It revealed that Ku70/Ku80 were notably enriched at DSB sites in control cells following DSB induction (Fig. 4d, e), while the reduced associations of Ku70/Ku80 were observed in *LRIK* knockdown cells (Fig. 4d, e). Correspondingly, the downstream factors, DNA-PKcs and XRCC4, also exhibited significant enrichment in control cells at an endogenous locus cut by AsiSI (Fig. 4f, g). However, impaired accumulation of DNA-PKcs and XRCC4 in cells was observed in *LRIK* knockdown cells (Fig. 4f, g). Hence, our results illustrate that the interaction of *LRIK* with the Ku heterodimer enhances repair complex formation at sites of DSBs in chromatin.

LRIK is required for efficient sensing and signaling of DSBs to promote the formation of γH2AX foci

Next, we investigated whether *LRIK* interacts with damaged DNA in DSB repair. After a 1-h recovery period following the phleomycin or doxorubicin treatments, the level of *LRIK* showed a significantly increase in the chromatin-associated fraction (Fig. 5a), suggesting that the majority of *LRIK* were fixed with chromatin in response to the DSB stress. To further test whether *LRIK* binds to DNA at the DNA damage sites during NHEJ repair, psoralen (AMT) cross-linked ChIRP (chromatin isolation and RNA purification) assays were performed. After introducing site-directed breaks by AsiSI, AMT was used to cross-link the RNA-bound DNA in vivo since it specifically cross-links direct RNA–DNA and RNA–RNA interactions. Chromatin was sonicated, and nucleosomes associated with *LRIK* were separated for further analysis. By examining the enrichment of two different DNA fragments, which are 2 Mbp and 60 bp away from the AsiSI-induced DSB site, respectively, the results revealed that *LRIK* interacts directly with DNA at the DSB damaged sites over non-DSB lesions (Fig. 5b, c).

Since *LRIK* is required for recruitment of DNA repair factors to DSBs, we speculated that failure to recruit DNA-PKcs in *LRIK* depleted cells may inhibit the formation of gamma H2AX foci. As expect, the levels of phosphorylated histone H2AX were impaired in *LRIK* knockdown cells compared with control (shNeg) cells following phleomycin treatment (Fig. 5d). Since phosphorylated histone H2AX (γH2AX) [38] is a critical marker in response to DSB formation [39], we further examined the localization of *LRIK* and γH2AX to check the localization of *LRIK* at DSB repair sites. By employing the FISH assay, we observed that the location of *LRIK* overlapped well with γH2AX in the nucleus after cells were treated with doxorubicin (Figs. 5e and S4d), suggesting that *LRIK* may participate in the signaling of DSB lesions.

To further test our hypothesis, we investigated whether the efficiency of DSB sensing and signaling is affected by *LRIK* through monitoring the formation of γH2AX foci. We observed that *LRIK* knockdown cells exhibited fewer γH2AX foci than control samples during a 2-h period following irradiation, particularly at 0.5 h (Fig. 5f, g). Consistently, significantly reduced γH2AX foci were observed in *LRIK* deficient cells compared with control cells (shNeg) at the indicated time points using the X-ray mimic drug phleomycin (Fig. 5h, i). This demonstrates that significant reduction of the cellular levels of *LRIK* impairs the formation of γH2AX foci, demonstrating that *LRIK* affects the sensing and signaling of DSB and the subsequent formation of γH2AX foci.

Phosphorylation of H2AX is indispensable for the formation of γH2AX foci, and this occurs during the DSB sensing and signaling event [38, 40, 41]. It has been suggested that H2AX can be phosphorylated by ATR, ATM, and DNA-PKcs in response to DNA damage, while ATM and DNA-PKcs contribute to H2AX phosphorylation in response to DSBs [42, 43]. To investigate the reasons for reduced H2AX phosphorylation in *LRIK* knockdown cells, we detected the mRNA levels and expression levels of ATM and ATR in these cells. We observed that knockdown of *LRIK* did not affect the transcription or expression of ATM and ATR (Supplementary Fig. S5b–d). Furthermore, western blotting analyses following the *LRIK* pull-down assays showed that *LRIK* does not interact with ATR or ATM in vitro (Supplementary Fig. S5e, f). In addition, *LRIK* deficiency did not change the protein level of DNA-PKcs in whole cell extracts (Supplementary Fig. S5a). Our data indicate that the impaired formation of γH2AX in *LRIK* knockdown cells is mainly caused by reduced recruitment of DNA-PKcs at DSB sites.

To further confirm that the interaction of *LRIK* and Ku heterodimer is crucial for the DSB sensing and signaling event, we examined whether knockdown of Ku70 and Ku80 recreates similar phenotypes to that observed in *LRIK* knockdown cells. Since the γH2AX foci formation is a consequence of efficient DSB recognition, it can be used as an indicator of the completed DSB sensing and signaling. Depletion of Ku70 or Ku80 impaired the efficiency of γH2AX foci formation after 2 h of recovery, following their treatment with phleomycin (Supplementary Fig. S6). We conclude that *LRIK* functions in the NHEJ repair pathway via its interaction with Ku heterodimer.

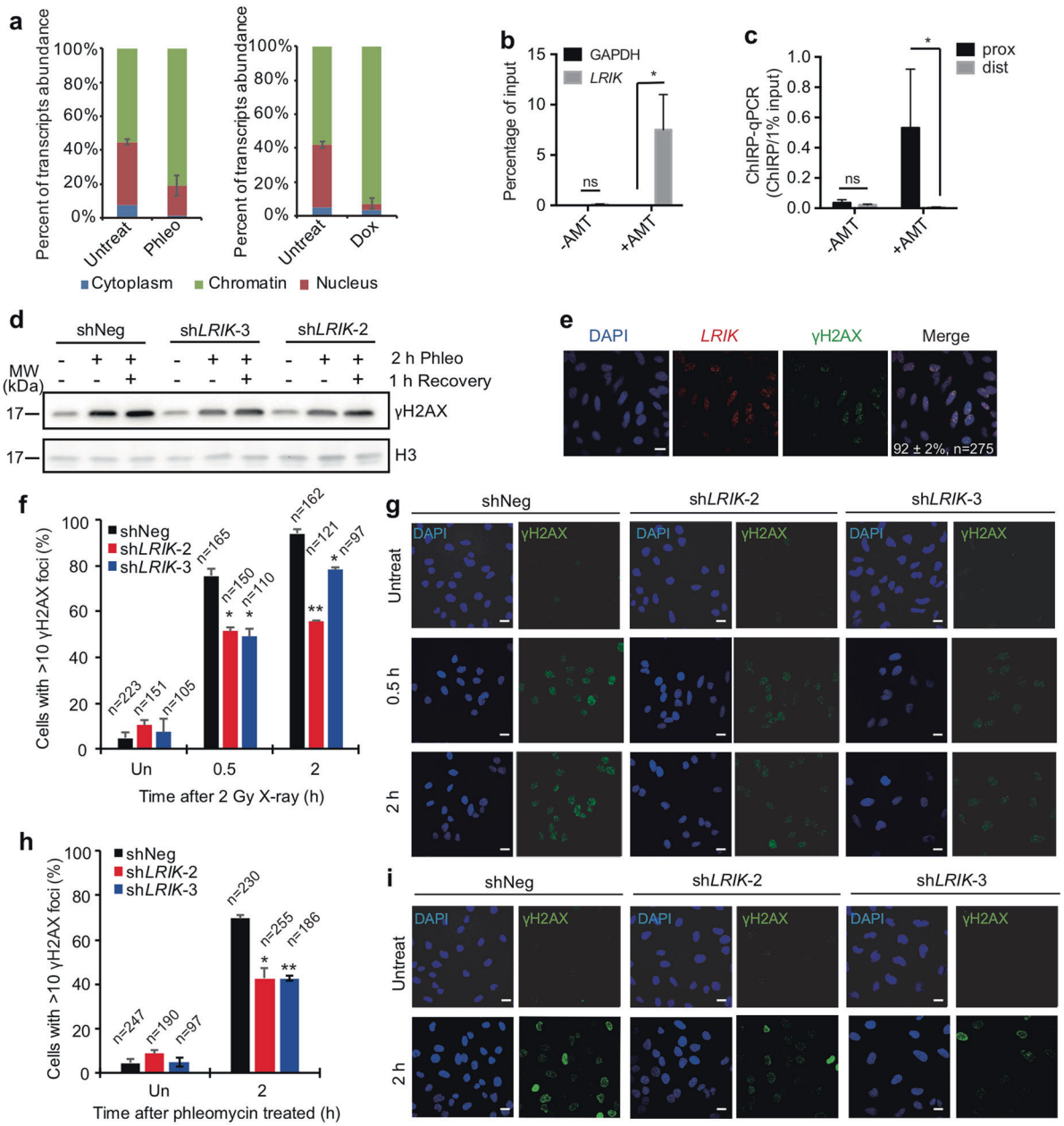

Fig. 5 ***LRIK*** **enhances the sensing and signaling of DNA double-strand breaks. a** Cellular distribution of *LRIK* measured by qRT-PCR in untreated cells or after recovery for 1 h following DSB-inducing agents treatments. Cytoplasm: cytoplasmic extracts, Nucleus: nuclear extracts, Chromatins: chromatin-associate components. The error bars indicate SD ($n = 3$ independent experiments). $^*P < 0.05$, $^{**}P < 0.01$, $^{***}P < 0.001$, by two-tailed Student's *t* test. **b** ChIRP-qPCR of *LRIK* in AMT cross-linked samples (+AMT) and no AMT cross-linked samples (−AMT). GAPDH served as a negative control. **c** Enrichment of *LRIK* binding on DNA double-strand breaks verified by ChIRP-qPCR detected with primers in the proximity or distal of the AsiSI-induced DSB. For (**b**, **c**), mean + SD, $n = 3$ independent experiments. $^*P < 0.05$, $^{**}P < 0.01$, $^{***}P < 0.001$, by two-way ANOVA. **d** Western blotting analyses of chromatin fractions showed that knockdown of *LRIK* impaired the level of γH2AX. The samples were extracted from cell lines with the same treatments described in Fig. 4a. **e** FISH images indicated that *LRIK* foci overlapped with γH2AX. HeLa cells were fixed after doxorubicin treatments for 2 h, and samples were immunostained with *LRIK* (red), γH2AX (green), and DAPI (blue). The percentage of *LRIK* co-localizing with γH2AX signal indicated was measured 275 cells from $n = 3$ independent experiments. Scale bar, 20 µm. **f** Immunofluorescence analyses of γH2AX foci indicated that *LRIK* knockdown cells exhibited impaired γH2AX foci formation. Quantitative measurements of γH2AX foci were performed following 2 Gy of X-ray irradiation and fixed at indicated times. Cells with >10 γH2AX foci were scored as positive. The error bars indicate SD ($n = 3$ independent experiments, the precise number of cells analyzed in total per condition was indicated). **g** The representative images of γH2AX foci in (**f**) are shown. Scale bar, 20 µm. **h** Immunofluorescence analyses of γH2AX foci indicated that *LRIK* knockdown cells exhibited impairment of γH2AX foci formation following their treatment of phleomycin. γH2AX foci were enumerated in tested samples. Cells with >10 γH2AX foci were scored as positive. The error bars indicate SD ($n = 3$ independent experiments, the precise number of cells analyzed in total per condition was indicated). **i** The representative images of γH2AX foci in (**h**) are shown. Scale bar, 20 µm. $^*P < 0.05$, $^{**}P < 0.01$, by two-tailed Student's *t* test.

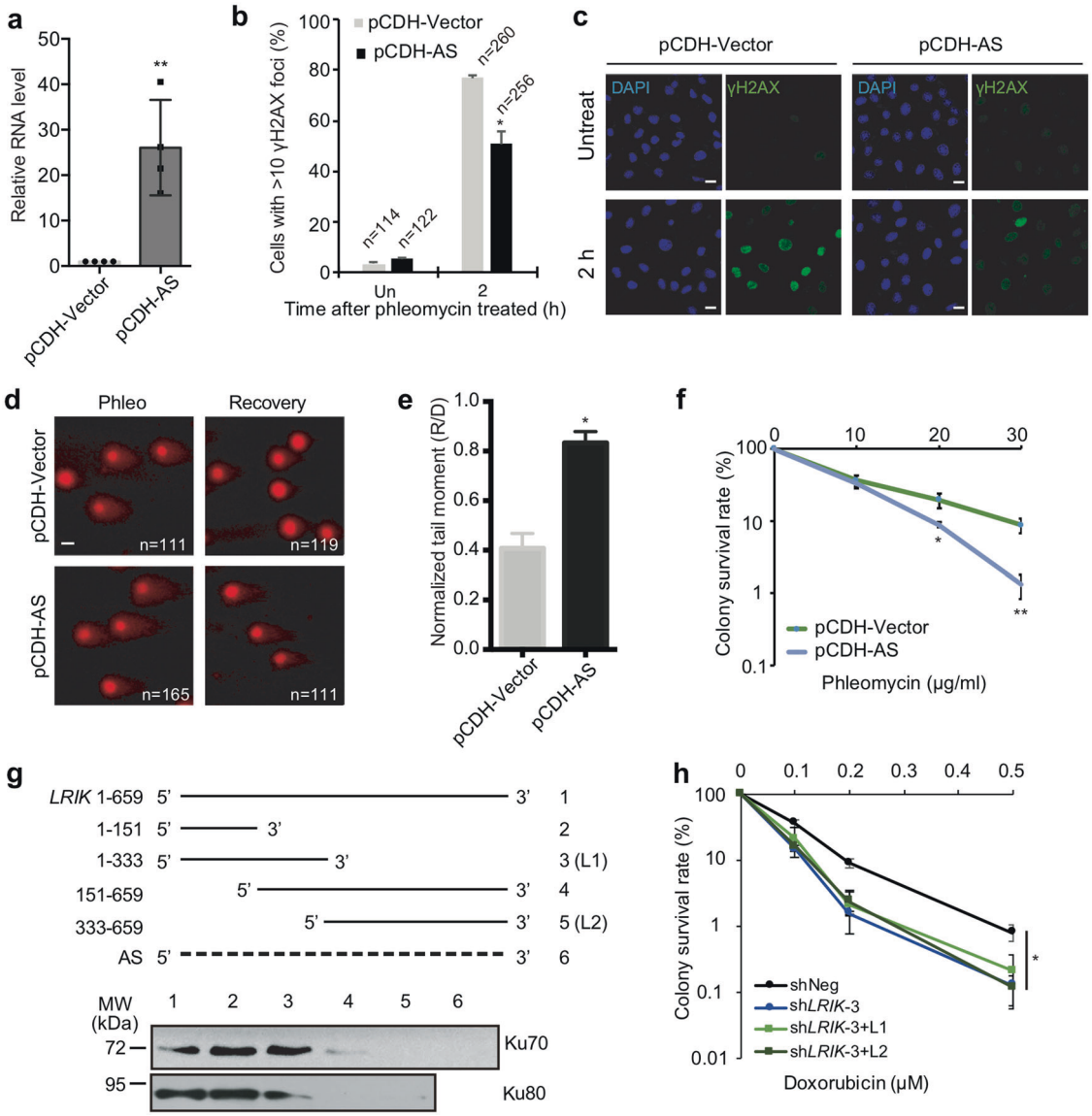

Fig. 6 Impeding the interaction of *LRIK* and Ku70 influences the efficient repair of DSB. a The expression level of antisense of *LRIK* determined by qRT-PCR. The error bars indicate SD ($n = 4$ independent experiments). **b** Immunofluorescence analyses of γH2AX foci indicated that expression of *LRIK* antisense impaired the γH2AX foci formation after recovery for 2 h following phleomycin treated. γH2AX foci were calculated in tested samples. Cells with >10 γH2AX foci were scored as positive. The error bars indicate SD ($n = 3$ independent experiments, the precise number of cells analyzed in total per condition was indicated). **c** Representative images of γH2AX foci. Scale bar 20 μm. **d** Typical images of comet assay revealed impaired DSB repair efficiency in *LRIK* antisense expression cells compared with control cells (the precise number of cells analyzed in total per condition was indicated). **e** Quantified tail moment of tested samples with CASP software showed significantly impaired DSB repair efficiency in *LRIK* antisense expression cells. Samples were treated with 20 μg/ml phleomycin for 2 h with or without recovering for another 2 h. The error bars indicate SD ($n = 3$ independent experiments, the precise number of cells analyzed in total per condition was indicated in (**d**)). **f** Colony-forming assays showed that cells with expression of *LRIK* antisense exhibited reduced survival rate after phleomycin treated. The error bars indicate SD ($n = 3$ independent experiments). $^{*}P < 0.05$, $^{**}P < 0.01$, by two-tailed Student's *t* test. **g** The sketch map of truncated *LRIK* used in pull-down assays. Bottom, western blot analyses of pull-down assays with truncated *LRIK* fragments indicated that the 5′ region of *LRIK* (1–151 nucleotides) mainly interacts with Ku. **h** Colony survival rates of overexpressing truncated *LRIK* in *LRIK* knockdown cells. L1: 1–333 nt of *LRIK*, L2: 333–659 nt of *LRIK*. The error bars indicate SD ($n = 3$ independent experiments).

Efficient DSB repair requires the interaction of *LRIK* and Ku heterodimer

To further confirm the coordinated function of *LRIK* and Ku heterodimer in DSBs repair particularly in the NHEJ repair pathway, a HeLa cell line expressing antisense of *LRIK* was constructed by transfecting a plasmid (pCDH-CMV-AS) in HeLa cells (Fig. 6a). It is exhibited that the γH2AX foci formation was impaired in *LRIK* antisense expression cells instead of control cells after recovery for 2 h following the

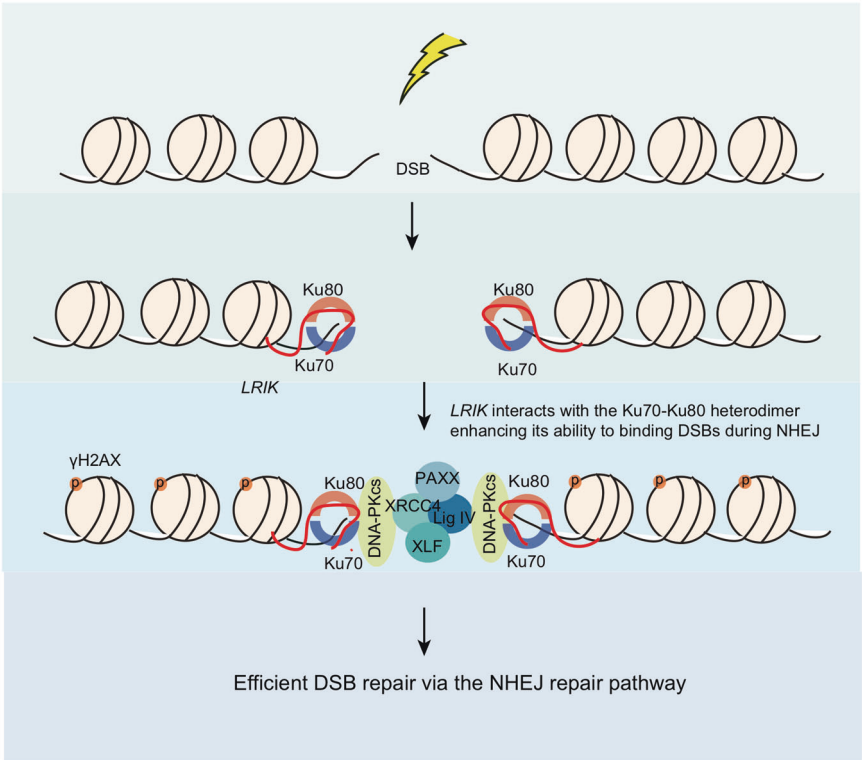

Fig. 7 Model of *LRIK* functioning in the NHEJ repair pathway. *LRIK* interacts with the Ku heterodimer thus promoting the occupancy of Ku with damaged chromatin, resulting in facilitating the assemblies of other downstream repair factors and promoting γH2AX foci formation, hence influences the efficient repair of DSBs.

phleomycin treatment (Fig. 6b, c). The DSB repair efficiency was reduced after hindering the interaction of *LRIK* and Ku70 through expressing antisense of *LRIK* measured with the neutral comet assays (Figs. 6d, e and S7a–c). Consistently, expression of antisense of *LRIK* caused significantly increased sensitivity to phleomycin (Fig. 6f), illustrating that *LRIK* and Ku70 function in NHEJ repair coordinately.

Finally, we sought to characterize the interacting regions of *LRIK* that associate with the Ku heterodimer. The Ku heterodimer binding capacity of different regions of *LRIK* in vitro demonstrated that the Ku heterodimer primarily binds with the 1–151 nucleotides region of *LRIK* (Fig. 6g). Moreover, the sensitivities of cells to the DSB-inducing agent were examined following truncated *LRIK* vectors overexpressed in *LRIK* knockdown cells. Interestingly, neither the 1–333 nt nor 333–659 nt regions of *LRIK* can rescue the sensitivity of *LRIK* knockdown cells (Fig. 6h). This demonstrates that the efficient repair of DSB requires intact *LRIK*.

Discussion

Despite the discovery of the versatile functions of lncRNAs having been reported [44], only a few lncRNAs have been implicated in the repair of DNA [5–9, 45]. Here, we identified and characterized a novel lncRNA *LRIK*, which functions during NHEJ repair and participates in repairing DSBs in human cells. Interacting with the Ku heterodimer, *LRIK* promotes the binding of the Ku heterodimer at DSB sites and facilitates the assemblies of the downstream repair factors that are required for the efficient sensing and repair DSBs (Fig. 7).

Publications have demonstrated that Ku70 exhibits a higher affinity binding to hairpin RNAs with certain structure than linear ssRNAs, dsRNAs, or other types of hairpin RNAs [46], for example, the bulge motif is essential for Ku binding RNAs like TLC1 [47]. Publications suggest that specific sequences of RNAs display high affinities with Ku70 [48], and these sequences (AATG, CATGA) have been found in *LRIK*. Besides, the other proteins identified by mass spectrometry showed no specific interaction with *LRIK* compared with Ku70 (Fig. 2d). Hence, it demonstrates that Ku70 selectively interacts with *LRIK* during the NHEJ repair.

Since the recognition of DNA lesions requires the prolonged association of DNA repair factors with DNA damaged sites [37], we hypothesized that *LRIK* assists Ku heterodimer during the DSB sensing and signaling event. Consistent with this notion, we observed that the occupancy of Ku70, Ku80, XRCC4, and DNA-PKcs with

chromatin was reduced in *LRIK* deficient cells after they were treated with DSB-inducing agents (Figs. 4 and S4), implying that *LRIK* may reinforce Ku70 binding with damaged chromatin. Our data show that *LRIK* interaction with Ku heterodimer results in prolonged association with DSB sites and the recruitment of XRCC4 and DNA-PKcs.

In summary, the formation of DSBs in cells induces *LRIK*, which together with the Ku heterodimer functions coordinately to enhance the signaling of DSBs by regulating the assembly of downstream repair factors on chromatin, thus enhancing the efficiency of DSB repair (Fig. 7). This study deepens our understanding of both lncRNA functioning and the sensing and signaling event of the NHEJ repair pathway that may pave the way for application in drug designation and cancer treatments.

Acknowledgements We thank Dr. Xiaowei Chen for discussion with microarray data as well as Dr. Xin Tong for technical support. We thank Dr. Patrick van Eijk for the critical comments. This work was supported by the National Natural Science Foundation of China (31520103905), the Hunan Science and Technology Program Fund (2014WK3021), and the National Key R&D Program of China (2017YFC0907503 and 2018YFA0106901).

Compliance with ethical standards

Conflict of interest The authors declare that they have no conflict of interest.

Publisher's note Springer Nature remains neutral with regard to jurisdictional claims in published maps and institutional affiliations.

References

1. Lord CJ, Ashworth A. The DNA damage response and cancer therapy. Nature. 2012;481:287–94.
2. Ciccia A, Elledge SJ. The DNA damage response: making it safe to play with knives. Mol Cell. 2010;40:179–204.
3. Rinn JL, Chang HY. Genome regulation by long noncoding RNAs. Annu Rev Biochem 2012;81:145–66.
4. Quinn JJ, Chang HY. Unique features of long non-coding RNA biogenesis and function. Nat Rev Genet. 2016;17:47–62.
5. Huarte M, Guttman M, Feldser D, Garber M, Koziol MJ, Kenzelmann-Broz D, et al. A large intergenic noncoding RNA induced by p53 mediates global gene repression in the p53 response. Cell. 2010;142:409–19.
6. Dimitrova N, Zamudio JR, Jong RM, Soukup D, Resnick R, Sarma K, et al. LincRNA-p21 activates p21 in cis to promote polycomb target gene expression and to enforce the G1/S checkpoint. Mol Cell. 2014;54:777–90.
7. Zhang A, Zhou N, Huang J, Liu Q, Fukuda K, Ma D, et al. The human long non-coding RNA-RoR is a p53 repressor in response to DNA damage. Cell Res. 2013;23:340–50.
8. Hung T, Wang YL, Lin MF, Koegel AK, Kotake Y, Grant GD, et al. Extensive and coordinated transcription of noncoding RNAs within cell-cycle promoters. Nat Genet. 2011;43:621–9.
9. Schmitt AM, Garcia JT, Hung T, Flynn RA, Shen Y, Qu K, et al. An inducible long noncoding RNA amplifies DNA damage signaling. Nat Genet. 2016;48:1370–6.
10. Shihabudeen Haider Ali MS, Cheng X, Moran M, Haemmig S, Naldrett MJ, Alvarez S, et al. LncRNA Meg3 protects endothelial function by regulating the DNA damage response. Nucleic Acids Res. 2019;47:1505–22.
11. Polo SE, Jackson SP. Dynamics of DNA damage response proteins at DNA breaks: a focus on protein modifications. Gene Dev. 2011;25:409–33.
12. Jackson SP, Bartek J. The DNA-damage response in human biology and disease. Nature. 2009;461:1071–8.
13. Spagnolo L, Rivera-Calzada A, Pearl LH, Llorca O. Three-dimensional structure of the human DNA-PKcs/Ku70/Ku80 complex assembled on DNA and its implications for DNA DSB repair. Mol Cell. 2006;22:511–9.
14. Rivera-Calzada A, Spagnolo L, Pearl LH, Llorca O. Structural model of full-length human Ku70-Ku80 heterodimer and its recognition of DNA and DNA-PKcs. EMBO Rep. 2007;8:56–62.
15. Gottlieb TM, Jackson SP. The DNA-dependent protein kinase: requirement for DNA ends and association with Ku antigen. Cell. 1993;72:131–42.
16. Zhang YY, He Q, Hu ZY, Feng Y, Fan LL, Tang ZQ, et al. Long noncoding RNA LINP1 regulates repair of DNA double-strand breaks in triple-negative breast cancer. Nat Struct Mol Biol. 2016;23:522–30.
17. Downs JA, Jackson SP. A means to a DNA end: the many roles of Ku. Nat Rev Mol Cell Bio. 2004;5:367–78.
18. Pfingsten JS, Goodrich KJ, Taabazuing C, Ouenzar F, Chartrand P, Cech TR. Mutually exclusive binding of telomerase RNA and DNA by Ku alters telomerase recruitment model. Cell. 2012;148:922–32.
19. Ting NS, Yu Y, Pohorelic B, Lees-Miller SP, Beattie TL. Human Ku70/80 interacts directly with hTR, the RNA component of human telomerase. Nucleic Acids Res. 2005;33:2090–8.
20. Chen HW, Xue J, Churikov D, Hass EP, Shi SH, Lemon LD, et al. Structural insights into yeast telomerase recruitment to telomeres. Cell. 2018;172:331.
21. Yan D, He D, He S, Chen X, Fan Z, Chen R. Identification and analysis of intermediate size noncoding RNAs in the human fetal brain. PLoS ONE. 2011;6:e21652.
22. Xie CY, Yuan J, Li H, Li M, Zhao GG, Bu DC, et al. NONCODEv4: exploring the world of long non-coding RNA genes. Nucleic Acids Res. 2014;42:D98–103.
23. Park C, Suh Y, Cuervo AM. Regulated degradation of Chk1 by chaperone-mediated autophagy in response to DNA damage. Nat Commun 2015;6:6823–37.
24. Tsai MC, Manor O, Wan Y, Mosammaparast N, Wang JK, Lan F, et al. Long noncoding RNA as modular scaffold of histone modification complexes. Science. 2010;329:689–93.
25. Xing Z, Lin A, Li C, Liang K, Wang S, Liu Y, et al. lncRNA directs cooperative epigenetic regulation downstream of chemokine signals. Cell. 2014;159:1110–25.
26. Xiang JF, Yin QF, Chen T, Zhang Y, Zhang XO, Wu Z, et al. Human colorectal cancer-specific CCAT1-L lncRNA regulates long-range chromatin interactions at the MYC locus (vol 24, pg 513, 2014). Cell Res. 2014;24:1150.
27. Tyteca S, Vandromme M, Legube G, Chevillard-Briet M, Trouche D. Tip60 and p400 are both required for UV-induced apoptosis but play antagonistic roles in cell cycle progression. Embo J. 2006;25:1680–9.
28. Xing YH, Yao RW, Zhang Y, Guo CJ, Jiang S, Xu G, et al. SLERT regulates DDX21 rings associated with Pol I transcription. Cell. 2017;169:664–78 e616.
29. Chu C, Quinn J, Chang HY. Chromatin Isolation by RNA Purification (ChIRP). J Vis Exp. 2012:e3912.
30. Shen CJ, Hsieh T, Wang JC, Hearst JE. Photochemical cross-linking of DNA-Rna helices by psoralen derivatives. J Mol Biol. 1977;116:661–79.

31. Chatterjee PK, Cantor CR. Preparation of psoralen-cross-linked R-loops and generation of large deletions by their repair in vivo. J Biol Chem. 1982;257:9173–80.
32. Ochi T, Blackford AN, Coates J, Jhujh S, Mehmood S, Tamura N, et al. DNA repair. PAXX, a paralog of XRCC4 and XLF, interacts with Ku to promote DNA double-strand break repair. Science. 2015;347:185–8.
33. Wang L, Park HJ, Dasari S, Wang S, Kocher JP, Li W. CPAT: Coding-Potential Assessment Tool using an alignment-free logistic regression model. Nucleic Acids Res. 2013;41:e74.
34. Sun L, Luo HT, Bu DC, Zhao GG, Yu KT, Zhang CH, et al. Utilizing sequence intrinsic composition to classify protein-coding and long non-coding transcripts. Nucleic Acids Res. 2013;41: e166.
35. Bennardo N, Cheng A, Huang N, Stark JM. Alternative-NHEJ is a mechanistically distinct pathway of mammalian chromosome break repair. PLoS Genet. 2008;4:e1000110.
36. Pierce AJ, Johnson RD, Thompson LH, Jasin M. XRCC3 promotes homology-directed repair of DNA damage in mammalian cells. Gene Dev. 1999;13:2633–8.
37. Soutoglou E, Misteli T. Activation of the cellular DNA damage response in the absence of DNA lesions (vol 320, pg 1507, 2008). Science. 2010;327:959.
38. Kinner A, Wu WQ, Staudt C, Iliakis G. Gamma-H2AX in recognition and signaling of DNA double-strand breaks in the context of chromatin. Nucleic Acids Res. 2008;36:5678–94.
39. Celeste A, Fernandez-Capetillo O, Kruhlak MJ, Pilch DR, Staudt DW, Lee A, et al. Histone H2AX phosphorylation is dispensable for the initial recognition of DNA breaks. Nat Cell Biol. 2003;5:675–9.
40. Keogh MC, Kim JA, Downey M, Fillingham J, Chowdhury D, Harrison JC, et al. A phosphatase complex that dephosphorylates gamma H2AX regulates DNA damage checkpoint recovery. Nature. 2006;439:497–501.
41. Lobrich M, Shibata A, Beucher A, Fisher A, Ensminger M, Goodarzi AA, et al. Gamma H2AX foci analysis for monitoring DNA double-strand break repair strengths, limitations and optimization. Cell Cycle. 2010;9:662–9.
42. Miller KM, Jackson SP. Histone marks: repairing DNA breaks within the context of chromatin. Biochem Soc Trans. 2012;40:370–6.
43. Jazayeri A, Falck J, Lukas C, Bartek J, Smith GCM, Lukas J, et al. ATM- and cell cycle-dependent regulation of ATR in response to DNA double-strand breaks. Nat Cell Biol. 2006;8:37–45.
44. Zhao Y, Li H, Fang S, Kang Y, Wu W, Hao Y, et al. NONCODE 2016: an informative and valuable data source of long non-coding RNAs. Nucleic Acids Res. 2016;44:D203–8.
45. Liu X, Li D, Zhang W, Guo M, Zhan Q. Long non-coding RNA gadd7 interacts with TDP-43 and regulates Cdk6 mRNA decay. EMBO J. 2012;31:4415–27.
46. Anisenko AN, Knyazhanskaya ES, Zatsepin TS, Gottikh MB. Human Ku70 protein binds hairpin RNA and double stranded DNA through two different sites. Biochimie. 2017;132:85–93.
47. Dalby AB, Goodrich KJ, Pfingsten JS, Cech TR. RNA recognition by the DNA end-binding Ku heterodimer. RNA. 2013;19:841–51.
48. Yoo S, Dynan WS. Characterization of the RNA binding properties of Ku protein. Biochemistry. 1998;37:1336–43.